Random sequential adsorption of Platonic and Archimedean solids

Piotr Kubala*

M. Smoluchowski Institute of Physics, Department of Statistical Physics, Jagiellonian University, 30-348 Kraków, Poland

(Received 5 June 2019; revised manuscript received 10 August 2019; published 8 October 2019)

The aim of this study is the analysis of packings generated according to random sequential adsorption protocol consisting of identical Platonic and Archimedean solids. The computer simulations performed showed that the highest saturated packing fraction $\theta = 0.402\,10(68)$ is reached by packings build of truncated tetrahedra and the smallest one $\theta = 0.356\,35(67)$ by packings composed of regular tetrahedra. The propagation of translational and orientational order exhibited microstructural properties typically seen in random sequential adsorption packings and the kinetics of three-dimensional packings growth were again observed not to be strictly connected with the dimension of the configuration space. Moreover, a fast overlap criterion for Platonic and Archimedean solids based on separating axis theorem has been described. The criterion, together with other optimizations, allowed us to generate significantly larger packings, which translated directly to a lower statistical error of the results obtained. Additionally, the polyhedral order parameters provided can be utilized in other studies regarding particles of polyhedral symmetry.

DOI: 10.1103/PhysRevE.100.042903

I. INTRODUCTION

Packings of objects are a mature field of theoretical, numerical, and experimental studies, dating back to ancient times. The problem of effective transportation of cannonballs on ships in colonial era aroused high interest among mathematicians of that time. The first problem of this kind, examined by Thomas Harriot around 1587, was the so-called *cannonball problem*—how many cannonballs can be arranged in both a square and a pyramid with a square base; in other words: which squares of natural numbers are also pyramidal numbers, which can be reexpressed as diophantic equation $k(k+1)(2k+1)/6 = n^2$ with the smallest solution $k = 24$, $n = 70$. Only in 1918 did George Neville Watson prove, that there are no other solutions of this equation [1]. Formulating problems regarding packings is surprisingly easy; however, solving them tends to be highly complicated. Johannes Kepler was seeking the most optimal way to pack cannonballs. He conjectured that the densest packing possible of packing density $\pi/\sqrt{18} \approx 0.74$ is achieved by fcc lattice arrangement [2]. Two hundred years later Carl Friedrich Gauss made a step toward a proof by showing, that fcc packing of balls is the most optimal Bravais lattice packing [3]. Only in 2017 was the strict, complete proof presented by a mathematical group lead by Thomas Hales that this is the global maximum [4].

Nowadays, maximal packings are made use of in a variety of science fields, from condensed matter physics, where they model crystalline structures [5], to telecommunication, where they indicate how to optimize transfer rates [6]. Recent works incorporate various shapes, for example, Platonic and Archimidean solids [7] or two-parameter families of polyhedra [8]. Apart from maximal packings, extensive studies of random packings are being conducted, especially regarding the so-called random close packings (RCP), because their structure resembles one of liquid crystals, amorphous media, granular matter, and various biological systems [9]. The term *random* implies the lack of order, while *close packing* means that the neighboring particles are in contact and continuation of the process which has been used to obtain the packing (e.g., shaking or tapping the containter) no longer increases the packing density. However, as shown by Torquato [10], the definition of RCP cannot be made mathematically precise and basic properties, such as packing fraction, are highly sensitive to the type of numerical or experimental protocol, which was used to generate them.

This study focuses on a slightly different class of random packings, which, contrary to RCP, have well-defined mean values. They are obtained as a result of the so-called random sequential adsorption (RSA). It is a simple protocol, which consists of subsequent iterations of the following steps:

(i) The position and orientation of a trial object are selected randomly.

(ii) If it does not overlap with any of previously placed objects, then it is added to the packing and its position and orientation remain unaltered to the end of the process.

(iii) If it does overlap, then it is removed and abandonded.

The packing is called saturated, when there is no space left for placing any other particles. Historically, the first person to present the RSA model was Flory, who analyzed the statistics of adjacent pendant groups on long chains of vinyl polymers [11]. It corresponds to one-dimensional (1D) RSA, the mean saturated packing fraction of which was analytically calculated by Renyi's as a solution to the so-called *car parking problem* [12]. RSA is most commonly utilized in two dimensions [13–15], because it models monolayers obtained in irreversible adsorption process [13].

Three-dimensional RSA packings appear notably more rarely, because there is no physical realization of that process—it is unclear how a new particle could be placed

*pkua.log@gmail.com

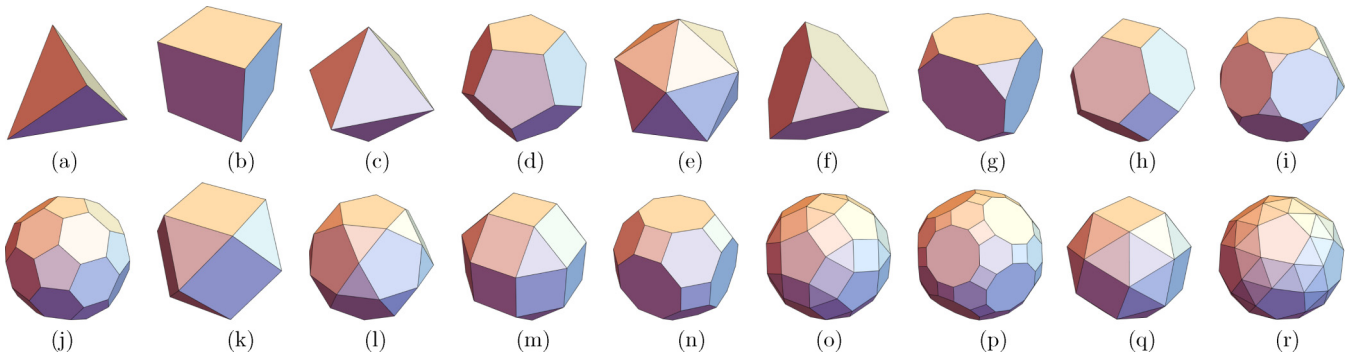

FIG. 1. All Platonic and Archimedean polyhedra: (a) regular tetrahedron, (b) cube, (c) r. octahedron, (d) r. dodecahedron, (e) r. icosahedron, (f) truncated tetrahedron, (g) truncated cube, (h) truncated octahedron, (i) truncated dodecahedron, (j) truncated icosahedron, (k) cuboctahedron, (l) icosidodecahedron, (m) rhombicuboctahedron, (n) truncated cuboctahedron, (o) rhombicosidodecahedron, (p) truncated icosidodecahedron, (q) snub cube, and (r) snub dodecahedron.

into the packing, which is already occupied by other particles, and stay in the place of addition. However, three-dimensional models are essential to understand RSA process. They can also be used as a toy model for other kinds of packings, because they share common properties with them, for example, maximas of density of speroid packings are achieved by similar particle dimensions both for RSA [16] and RCP [17] packings. There are numerical studies regarding RSA packings of spheres [18], spheroids [16], unoriented cubes [19] and cuboids [20,21] as well as oriented hypercubes in the context of Palasti conjecture [22,23].

The natural continuation of three-dimensional RSA studies are Platonic and Archimedean solids (see Fig. 1). The main goal of this study is to find the mean saturated packing fraction of all 18 polyhedra and to analyze how it is influenced by the solids' shape. RSA packings of those solids are also interesting in terms of the kinetics of packing growth, which, as presented later, have been lately discovered to be more complex than what had been previously believed. Moreover, it will also be interesting to compare the result with the recent studies regarding maximal packings [7].

The paper is divided into four sections. Section II presents the details of computer simulations performed. Section II A describes their parameters and gives a brief discussion on rotations sampling. Section II B is devoted to a fast overlap test for Platonic and Archimedean solids which can be generalized to other convex polyhedra. Section II C indicates where additional optimizations that can be made are described. Section III A presents the method to estimate saturated packing fractions and lists their values. Section III B discusses the kinetics of packing growth, and then Sec. III C elaborates on the correlation between packing fraction and the shape of solids. Section III D describes the microstructural properties of packings in terms of the propagation of translational and orientational order. It presents orientational order parameters conforming to point groups of polyhedral symmetries. Section IV briefly summarizes the findings.

II. METHODS

A. Description of simulations

In order to study the properties of packings of Platonic and Archimedean solids, packings were generated numerically according to the RSA scheme described in the Introduction. For the sake of convenience all solids had a unit volume. The positions of their centers were selected randomly from a cube with the edge size of 50. In order to reduce finite-size effects, periodic boundary conditions were used. A brief discussion of errors connected with finite size is presented in Sec. III D.

Trial particles, oriented in the same way at the beginning, were rotated randomly in a way which assures that each final orientation is equally probable. A natural way to obtain uniform distribution of SO(3) rotations can be given by a probabilistic measure being translation-invariant Haar measure [as the SO(3) group is compact, the right and left Haar measures are equal]. It corresponds to the intuition that probability of choosing rotation from a measurable subset $A \subset \mathrm{SO}(3)$ should not change after a translation by an arbitrary rotation Γ: $P(R \in A) = P(R \in \Gamma A)$. The details of this reasoning can be found in Ref. [24]. One way of obtaining such a distribution is the composition of three rotations

$$R = R_3 R_2 R_1, \tag{1}$$

where R_1, R_2, R_3 are rotations around consecutive coordinate system axes by, respectively, $2\pi x_1$, $\arcsin(2x_2 - 1)$ and $2\pi x_3$ radians, where x_1, x_2, x_3 are random numbers from Unif(0, 1) distribution. In Ref. [15] it was shown that for such a way of sampling orientations, the correlations of orientations decay to 0 for large-enough distances, which is additional, numerical argument for the correctness of that choice.

The main parameter tracked during simulation was the packing fraction defined as

$$\theta(t) = \frac{N(t)V}{V_C} = \frac{N(t)}{V_C}, \tag{2}$$

where $V = 1$ is the particle's volume, $V_C = 50^3$ is the system volume, and $N(t)$ is the number of particles in the packing after dimensionless time t. Dimensionless time is defined as

$$t = \frac{nV}{V_C} = \frac{n}{V_C}, \tag{3}$$

where n is the number of RSA iterations. Dimensionless time is often used to compare the results regardless of V and V_C.

The packing becomes saturated when there is no possibility of adding another object. The mean saturated packing fraction

θ depends only on particle's shape and, contrary to RCP, the mean value is well defined.

For practical reasons, one does not usually generate saturated packings since there is no general method to detect whether a packing is already saturated or not. Hence, in this study packing generation was stopped after arbitrarily chosen time $t = 10^6$ which corresponds to 1.25×10^{11} RSA algorithm iterations. This value is a trade-off between the accuracy of estimation of saturated state properties and computational time.

For each solid 100 independent packings were generated, which gives a few millions of particles in total. As it will be discussed later, it was enough to yield statistical error of mean packing fraction after $t = 10^6$ one order lower than the uncertainty introduced by extrapolation to the saturated state.

B. Overlap detection

Detecting overlaps of Platonic and Archimedean polyhedra is the most time-consuming operation during RSA packing generation. The choice of the fastest overlap detection algorithm shortens the simulation time significantly and effectively enables obtaining better statistics. In case of polyhedra, commonly used algorithm, especially in computer graphics, is triangulating their surface and testing triangle pairs against intersection. There exist fast triangle-triangle collision tests, such as in Ref. [25]. However, it was shown in Ref. [20] that in the case of cuboids another test—based on separating axis theorem—can be up to 100 times faster.

Separating axis theorem (SAT) [26] asserts that two convex multidimensional sets are disjunctive if and only if there exists such an axis that projections of these sets on it are disjunctive. This axis is then called separating axis, hence the theorem name. The theorem does not provide any information how to find this separating axis. It turns out, however, that in case of 3D polyhedra, such an axis does not exist if none of the axes perpendicular to faces of any polyhedron or perpendicular to two edges, each from one polyhedron, is a separating axis.

Let $\mathbf{P}_1, \ldots, \mathbf{P}_n$ be the positions of vertices of polyhedron P and $\mathbf{u}$ the normalized vector spanning potential separating axis. The direct way to check whether projections of convex polyhedra P and Q onto $\mathbf{u}$ overlap is to check the sing of the expression

$$\max\left\{\min_i\{\mathbf{P}_i\cdot\mathbf{u}\},\min_j\{\mathbf{Q}_j\cdot\mathbf{u}\}\right\} - \min\left\{\max_i\{\mathbf{P}_i\cdot\mathbf{u}\},\max_j\{\mathbf{Q}_j\cdot\mathbf{u}\}\right\}. \tag{4}$$

If it is positive, then projections are disjunctive and if it is negative, then they overlap. Zero value corresponds to tangent projections. Gottschalk proposed an optimization of this criterion for cuboids which enables us to calculate all projections in one step [26]. It can be easily generalized for sufficiently regular polyhedra.

Assume that eight vertices of a polyhedron form a cuboid or four vertices form a rectangle. Let one choose the origin and coordinate system axes $\hat{\mathbf{e}}_1$, $\hat{\mathbf{e}}_2$, $\hat{\mathbf{e}}_3$ so that coordinates of those vertices are $(\pm a, \pm b, \pm c)$, allowing one of a, b, c to be zero to include the case of the rectangle. It is easy to notice that the half length of a cuboid or rectangle projection onto $\mathbf{u}$ is then

$$\begin{aligned} L_C(\mathbf{u}) &= a|u^1| + b|u^2| + c|u^3| \\ &= a|\mathbf{u}\cdot\hat{\mathbf{e}}_1| + b|\mathbf{u}\cdot\hat{\mathbf{e}}_2| + c|\mathbf{u}\cdot\hat{\mathbf{e}}_3|. \end{aligned} \tag{5}$$

All achiral Platonic and Archimedean solids with octahedral or icosahedral symmetry are built exclusively of concentric, identically oriented groups of vertices arranged in cuboids or rectangles—it is due to the fact that both full (achiral) octahedral and icosahedral point groups contain rotations around three perpendicular twofold axes and reflections through three planes spanned by them. It reduces calculation of half length L_P of the polyhedron P to selecting maximal L_C. Then one can test a potential separating axis for solids P and Q with centers $\mathbf{O_P}$ and $\mathbf{O_Q}$ by checking the sign of the expression

$$|(\mathbf{O_Q}-\mathbf{O_P})\cdot\mathbf{u}| - \left[\max_{C_i\subset P}\{L_{C_i}(\mathbf{u})\} + \max_{C_j\subset Q}\{L_{C_j}(\mathbf{u})\}\right]. \tag{6}$$

Due to this optimization one can significantly reduce the number of calculations performed in an overlap test.

C. Additional optimizations

Although iterating the RSA steps described in the Introduction without any modifications is enough to obtain RSA packings, several optional optimizations can be made to increase the speed of packing generation, allowing us to obtain better statistic within the same computational time frame. For example, one can utilize the so-called modified RSA using exclusion zones to reduce the space from which new particles are selected or neighbor lists of adjacent particles to reduce the number of collision tests. To preserve the compact form of the paper these technical details have been omitted; however, they can be found in Ref. [18]. Although the RSA protocol is serial in nature, some parts of the simulation, for example, sampling new particles, can be done in parallel. It is discussed in detail in Ref. [27].

III. RESULTS

A. Packing fraction estimation

Determination of a moment when a packing becomes saturated requires tracking of regions not covered by shapes' excluded volumes. Recently, two independent algorithms for 2D shapes—[28] for polygons and [27,29] for ellipses, spherocylinders, and rectangles—have been proposed; however, there is no known generalization in higher dimensions. In case of spheres one can use the Feder's law [13,30] to extrapolate finite-time simulations to infinite time:

$$\theta - \theta(t) = At^{-\frac{1}{d}}. \tag{7}$$

It is valid for large-enough times where d is the packing dimension and A is a constant. Numerous studies, both analytical [31,32] and numerical [15,21], have shown that this relation holds for most anisotropic shapes but with different values of d. Equation (7), after substituting (2) and differentiating with respect to t, can be rewritten as $\ln(dN/dt) = \ln(AV_C/d) - (1/d+1)\ln(t)$, so d can be determined from linear fit to points $[\ln t, \ln dN/dt]$ (see Fig. 3). Here the fit was made for $t \in [10^4, 10^6]$. Then substituting $y = t^{-(1/d)}$ gives

TABLE I. Extrapolated saturated packing fractions together with corresponding d parameters and sphericity Ψ. The values for sphere are taken from Ref. [18]. The errors of packing fraction shown are errors propagated from errors of fits. The standard deviation of mean packing fraction after $t = 10^6$ was one order of magnitude smaller, so it was not taken into account.

Polyhedron name	θ	d	Ψ
tr. tetrahedron	0.402 10(68)	7.631(93)	0.775
tr. cuboctahedron	0.396 31(30)	6.882(75)	0.943
tr. icosidodecah.	0.393 10(27)	6.599(87)	0.970
snub cube	0.391 33(30)	7.235(92)	0.965
tr. octahedron	0.390 32(32)	6.641(71)	0.910
cuboctahedron	0.390 32(28)	6.681(58)	0.905
snub dodecahedron	0.389 78(24)	6.320(92)	0.982
icosidodecahedron	0.389 22(32)	6.426(89)	0.951
rhombicuboctah.	0.386 55(32)	7.080(98)	0.954
rhombicosidodecah.	0.386 40(22)	6.102(89)	0.979
tr. icosahedron	0.386 10(25)	6.609(90)	0.967
tr. dodecahedron	0.385 49(22)	5.930(57)	0.926
icosahedron	0.384 97(30)	6.443(81)	0.939
sphere	0.384 130 7(21)	3.073 046(17)	1.000
truncated cube	0.380 75(21)	5.827(43)	0.849
octahedron	0.379 82(38)	6.737(70)	0.846
dodecahedron	0.379 36(28)	6.197(71)	0.910
cube	0.362 49(27)	6.037(53)	0.806
tetrahedron	0.356 63(67)	8.119(93)	0.671

$\theta(y) = \theta - Ay$, so θ is then finally given by intersection of fit to $\theta(y)$ with the y axis.

The estimated saturated packing fractions are shown in Table I. Moreover, the example packings of size $10 \times 10 \times 10$ are shown in Fig. 2 and 3D models of them can be found in the Supplemental Material [33]. The least dense packings are made of regular tetrahedra, $\theta = 0.356\,63(67)$, and the most dense are made of truncated tetrahedra, $\theta = 0.402\,10(68)$. To put it in a context, the mean saturated packing fraction of spheres is $\theta = 0.384\,130\,7(21)$ placing between them. The errors given are propagated from linear regressions described above. The statistical errors of mean packing fractions before extrapolation have been neglected as they are one order lower. The new results for cubes differ from the previous ones [19] on the third decimal digit by the value slightly larger than the tolerance threshold 3σ, for both θ and d. That study utilized smaller simulation time $t = 10^5$ which can be the source of the difference.

B. The kinetics of packing growth

In papers regarding RSA of cubic shapes [19–21] one observes the deviation from a typical interpretation of d parameter as the dimension of configuration space. This dimension is equal to 6 in case of all 3D solids without axial symmetry, cuboids, Platonic and Archimidean solids included, while the reported values of d can be as high as 9. The values of parameter d here, when fitting to $t \in [10^4,\ 10^6]$, are for most shapes higher than 6, peaking to 8.119(93) for tetrahedron. For some shapes, namely rhombicosidodecahedron, truncated dodecahedron, and cube, they are close to 6 with respect to standard deviation. Apart from having the strong dependence

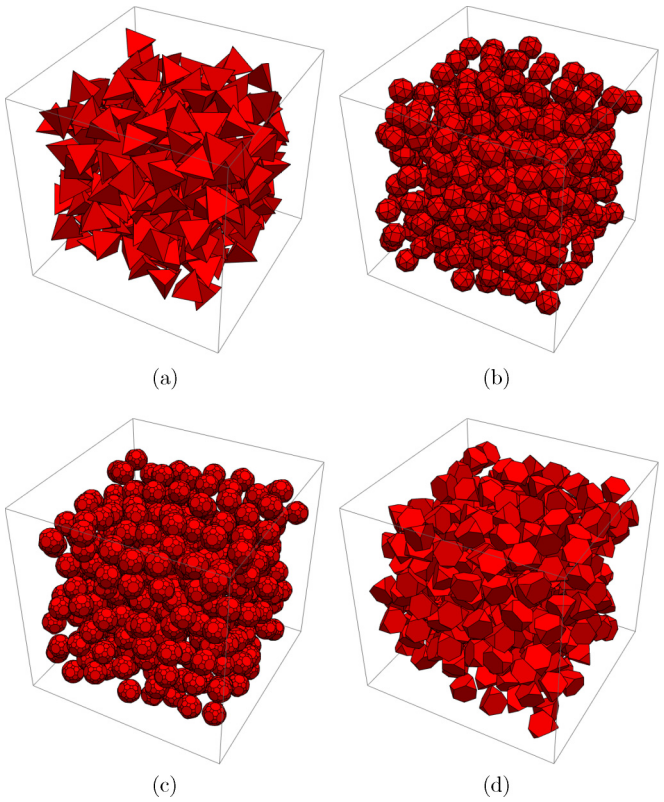

FIG. 2. Almost saturated packings of chosen polyhedra of size $10 \times 10 \times 10$. (a) Tetrahedron, (b) snub cube, (c) truncated icosidodecahedron, (d) truncated tetrahedron.

on particle shape, the d values seem to differ when fitting to different ranges of t (see Fig. 3, inset) and it remains unknown whether they can ever stabilize. This suggests that the estimated packing fractions can carry systematic errors connected with using slightly shifted d values in extrapolation. Unfortunately, there is no known way of determining their magnitude. There were attempts to use more sophisticated extrapolation models than the Feder's law [34]; however, they did not render different θ values, so the simple power fit remains the best approximation. To give the definite values of saturated

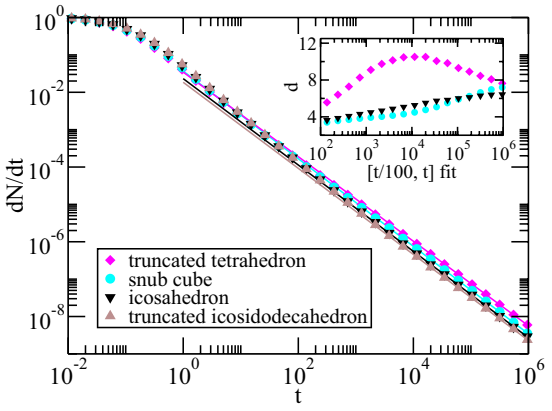

FIG. 3. The dependence of dN/dt on dimensionless time t (points) with fits to range $[10^4, 10^6]$ (straight lines). Additionally, the inset shows the dependence of the obtained d on time when fitting to range $[t/100, t]$.

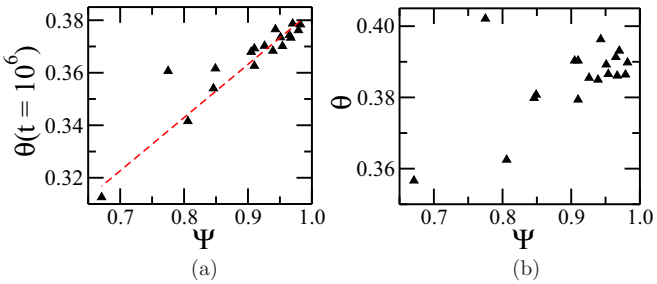

FIG. 4. The dependence of packing fraction θ on sphericity Ψ of Platonic and Archimedean solids. The left panel shows packing fractions after $t = 10^6$ and the right for saturated packings. The dashed line is a linear fit $\theta(t = 10^6) = 0.180\,82 + 0.202\,63\ \Psi$ to all points excluding truncated tetrahedron.

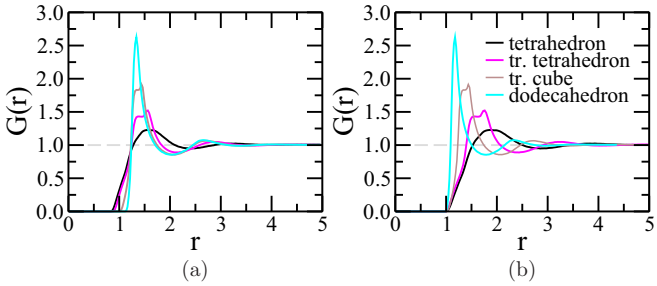

FIG. 5. The dependence of density pair correlation function on the distance between particles. Panel (a) shows real distances in simulations. In panel (b) they are normalized so that the smallest distance possible is equal to 1. The error bars are smaller than the width of the lines.

packing fractions and determine the exact asymptotic behavior, one needs to develop an algorithm allowing to generate saturated packings in three dimensions.

C. The influence of polyhedron shape on packing fraction

Known results for 2D and 3D shapes, such as rectangles [14,29], ellipses, spherocylinders (capsules) [15,27], dimers [15], spheroids [16], or cuboids [20,21], show that the packing fraction grows with the increase of anisotropy in the family of particles of a specific kind until it reaches maximum. In case of studied polyhedra one can see that geometric transformations, such as truncation, rectification, and expansion, transforming Platonic solids into Archimedean solids, increase the packing fraction. The most notable difference is for tetrahedron—after truncating the shape packed, packings become the most dense from the rarest of all analyzed. One has to notice that those transformations actually lower the sphericity of polyhedra, defined as [35]

$$\Psi = \frac{\pi^{\frac{1}{3}}(6V)^{\frac{2}{3}}}{A}, \tag{8}$$

which can be used as an indicator of particle anisotropy with volume V and area A. $\Psi \in (0, 1]$, and maximal value is reached only for sphere. Figure 4 shows the dependence of packing fraction on the sphericity of the studied polyhedra. Sphericity values are also included in Table I. The dependence of $\theta(t = 10^6)$ on Ψ resembles linear, with linear fit yielding $R^2 \approx 95\,\%$ having excluded truncated tetrahedron; however, after the extrapolation to $t = \infty$ the differences between points grow. The dependence is neither linear nor unimodal, which shows that a packing fraction θ for 3D particles strongly depends on the details of a particle shape. The last statement is supported even more strongly, having noted that the most densely packing shape—truncated tetrahedron—lies the farthest from presumptive trends for both time regimes thus its high packing fraction could not be predicted based solely on its sphericity value.

Densities of RSA packings of Platonic and Archimedean solids expose significant difference to maximal packings [7] in terms of shape dependence. For that type of packing, Platonic solids have generally higher densities than Archimedean, peaking at 1 for cube, which is different than for RSA packings, where the relation is opposite. On the other hand, tetrahedral shapes show alike behavior—the least dense maximal packing is for tetrahedron with $\theta = 0.782$ and truncated tetrahedron is one of the most tightly packing shapes with $\theta = 0.958$. Interestingly, the optimal Bravais lattice packing of tetrahedra has the density of $\theta = 0.367$ which is similar to RSA.

D. Microstructural properties

Apart from analyzing global packing parameters, such as packing fraction, one can also investigate into their microstructural properties. Here they were studied in terms of density pair correlation function and propagation of orientational order. The latter one required developing order parameters conforming to polyhedral point symmetries of Platonic and Archimedean solids.

1. Density correlation

The density pair correlation function is defined as [36]:

$$G(r) = \lim_{dr\to 0}\left\langle \frac{N(r, r+dr)}{4\pi r^2 \theta dr}\right\rangle, \tag{9}$$

where $N(r, r + dr)$ is the number of pairs whose distance is from $[r, r + dr]$ interval. Figure 5 shows $G(r)$ for chosen particle types. It presents behavior typically found in RSA packings—it decays superexponentially [36] with a series of maxima and minima. There are additional maxima for particles with nonequivalent faces, such as truncated tetrahedron. According to Ref. [37], $G(r)$ is strictly connected with an error in packing fraction introduced by finite-size effects, so, as there are almost no correlations after $r = 5$, finite-size effects should be negligible for a packing size used in this study.

2. Orientational order parameters

In order to measure full orientational order propagation, the order parameters conforming to polyhedral groups of point symmetries were used:

$$\rho_4(r) = \lim_{dr\to 0}\frac{9}{32}\left\langle \sum_{i,j}(\mathbf{u_i}\cdot\mathbf{v_j})^3\right\rangle_{[r,r+dr]}, \tag{10a}$$

$$\rho_8(r) = \lim_{dr\to 0}\frac{1}{6}\left\langle 5\left[\sum_{i,j}(\mathbf{u_i}\cdot\mathbf{v_j})^4\right] - 9\right\rangle_{[r,r+dr]}, \tag{10b}$$

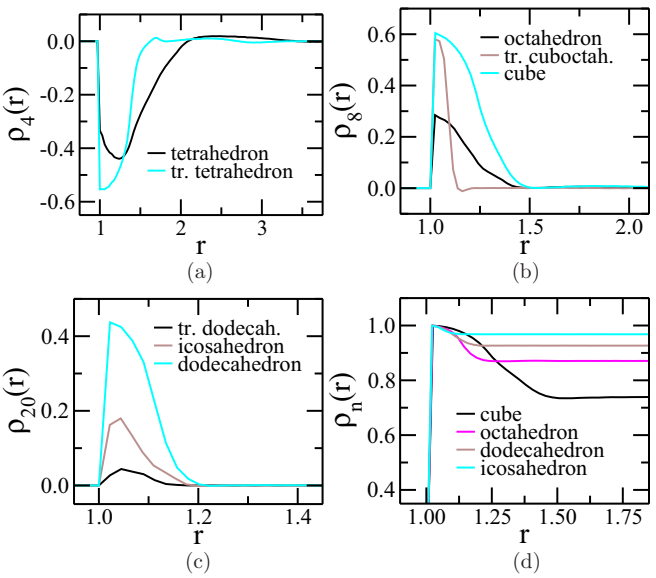

FIG. 6. [(a)–(c)] The dependence of polyhedral order ρ_x for chosen Platonic and Archimedean solids on the distance between their centers. The x axis is normalized in such a way that the smallest possible distance is 1. Additionally, panel (d) shows nematic order $\rho_n(r)$.

$$\rho_{20}(r) = \lim_{dr\to 0} \frac{25}{192} \left\langle 7\left[\sum_{i,j} (\mathbf{u_i}\cdot\mathbf{v_j})^6\right] - 36 \right\rangle_{[r,r+dr]}, \qquad (10c)$$

where ρ_4, ρ_8, and ρ_{20} are for, respectively, tetrahedral, octahedral, and icosahedral point groups. $\mathbf{u_i}$, $\mathbf{v_j}$ are the smallest sets of normalized equivalent rotational symmetry axes—namely three-, four-, and fivefold axes respectively—for two particles. The summation goes over all pairs of axes, each from one particle, and the average is calculated for all pairs of particles whose centers' distance is in the $[r, r+dr]$ interval. The exponents are even for symmetries where orientation of a particle is fully determined only by orientations of considered axes and odd where both orientation and sense of axes is needed. The values of the exponents are the smallest for which the sum is not constant regardless of particles' orientations. The appropriate linear normalization ensures that the value of these order parameters is 0 for isotropic ensemble of particles and 1 for identically oriented particles. For ρ_4 only, the normalization depends on the individual choices of sense of each of four axes—here it has been assumed that the ends of axes form regular tetrahedron when the beginnings are in the same point. It is also worth noting that ρ_4, ρ_8, ρ_{20} parameters are suitable for point groups both with and without reflections, namely for both chiral and achiral particles.

One can also check nematic order, using the standard P_1 and P_2 parameters

$$\rho_n(r) = \lim_{dr\to 0} \left\langle P_m\left(\max_{i,j}\{|\mathbf{u_i}\cdot\mathbf{v_j}|\}\right)\right\rangle_{[r,r+dr]}; \qquad (11)$$

however, in order to take degenerate axes into account, one has to check all pairs and choose the dot product with the maximal absolute value. The side effect of this operation is that ρ_n is not zero even for isotropic set. P_2 is used when both senses of axis are equivalent and P_1 when not. Nematic order parameters are suitable for Platonic solids, because they have one class of characteristic axes, which go through the middle of the faces. For Archimedean solids the choice is ambiguous.

The dependence of full order parameters on distance is shown in Figs. 6(a)–6(c). Is is typical for RSA packings. The highest order is seen for almost touching particles, where their faces have to be aligned to prevent an overlap; however, full order is never achieved. It is due to the fact that aligned particles still have rotational freedom around the normal axis of close faces. Nematic order parameters (d) confirm full nematic order for small distances. Both full and nematic order parameters decay quickly with a distance, which is also typical for RSA packings [38].

IV. SUMMARY

In this study RSA packings of five Platonic and thirteen Archimedean solids were examined. It has been shown that the loosest packings are formed by tetrahedra with packing fraction $\theta = 0.356\,63(67)$ and the densest are made of truncated tetrahedra with packing density of $\theta = 0.402\,10(68)$. In general, Archimedean solids form denser packings than Platonic solids; however, exact θ values depend strongly on particle shape, not only on sphericity Ψ. For the majority of the polyhedra studied the exponent d describing packing growth kinetics is not equal to configuration space dimension; however, one needs to generate strictly saturated packings to give the definite answer. There was no global translational or orientational order observed. Additionally, rapid intersection tests and order parameters conforming to polyhedral symmetries have been developed.

ACKNOWLEDGMENTS

This work was supported by Grant No. 2016/23/B/ST3/01145 of the National Science Center, Poland. Numerical simulations were carried out with the support of the Interdisciplinary Center for Mathematical and Computational Modeling (ICM) at the University of Warsaw under Grant No. G-27-8.

[1] G. Watson, Mess. Math **48**, 1 (1918).
[2] J. Kepler, *The Six-cornered Snowflake* (Paul Dry Books, Philadelphia, USA, 2010).
[3] C. F. Gauss, Gottingsche Gelehrte Anzeigen **1**, 169 (1831).
[4] T. Hales *et al.*, Forum of mathematics, Pi **5**, e2 (2017).
[5] Y. Kallus and V. Elser, Phys. Rev. E **83**, 036703 (2011).
[6] E. Agrell and M. Karlsson, J. Lightwave Technol. **27**, 5115 (2009).

[7] S. Torquato and Y. Jiao, Nature **460**, 876 (2009).
[8] E. R. Chen, D. Klotsa, M. Engel, P. F. Damasceno, and S. C. Glotzer, Phys. Rev. X **4**, 011024 (2014).
[9] S. Torquato and F. H. Stillinger, Rev. Mod. Phys. **82**, 2633 (2010).
[10] S. Torquato, T. M. Truskett, and P. G. Debenedetti, Phys. Rev. Lett. **84**, 2064 (2000).
[11] P. J. Flory, J. Am. Chem. Soc. **61**, 1518 (1939).
[12] A. Rényi, Publ. Math. Inst. Hung. Acad. Sci. **3**, 109 (1958).
[13] J. Feder, J. Theor. Biol. **87**, 237 (1980).
[14] R. D. Vigil and R. M. Ziff, J. Chem. Phys. **91**, 2599 (1989).
[15] M. Cieśla, G. Pająk, and R. M. Ziff, J. Chem. Phys. **145**, 044708 (2016).
[16] J. Sherwood, J. Phys. A: Math. Gen. **30**, L839 (1997).
[17] A. Donev, F. H. Stillinger, P. M. Chaikin, and S. Torquato, Phys. Rev. Lett. **92**, 255506 (2004).
[18] G. Zhang and S. Torquato, Phys. Rev. E **88**, 053312 (2013).
[19] M. Cieśla and P. Kubala, J. Chem. Phys. **148**, 024501 (2018).
[20] P. Kubala and M. Cieśla, Acta Phys. Polon. B **49**, 981 (2018).
[21] M. Cieśla and P. Kubala, J. Chem. Phys. **149**, 194704 (2018).
[22] $\theta_d = (\theta_1)^d$, where θ_d is mean saturated packing density of oriented d-dimensional hypercube RSA packings, so in particular θ_1 is the packing density in *car packing problem*.
[23] B. Bonnier, J. Phys. A: Math. Gen. **34**, 10757 (2001).
[24] R. E. Miles, Biometrika **52**, 636 (1965).
[25] T. Möller, J. Graph. Tools **2**, 25 (1997).
[26] S. Gottschalk, M. C. Lin, and D. Manocha, in *Proceedings of the 23rd Annual Conference on Computer Graphics and Interactive Techniques* (ACM, New York, 1996), pp. 171–180.
[27] K. Haiduk, P. Kubala, and M. Cieśla, Phys. Rev. E **98**, 063309 (2018).
[28] G. Zhang, Phys. Rev. E **97**, 043311 (2018).
[29] W. Kasperek, P. Kubala, and M. Cieśla, Phys. Rev. E **98**, 063310 (2018).
[30] Y. Pomeau, J. Phys. A: Math. Gen. **13**, L193 (1980).
[31] J. Talbot, G. Tarjus, and P. Schaaf, Phys. Rev. A **40**, 4808 (1989).
[32] A. Baule, Phys. Rev. Lett. **119**, 028003 (2017).
[33] See Supplemental Material at http://link.aps.org/supplemental/10.1103/PhysRevE.100.042903 for STL and Mathematica notebook files containing 3D figures of the packings.
[34] M. Cieśla, P. Kubala, and W. Nowak, Physica A **527**, 121361 (2019).
[35] H. Wadell, J. Geol. **43**, 250 (1935).
[36] B. Bonnier, D. Boyer, and P. Viot, J. Phys. A: Math. Gen. **27**, 3671 (1994).
[37] M. Cieśla and R. M. Ziff, J. Stat. Mech. (2018) 043302.
[38] M. Cieśla and J. Barbasz, Colloids Surf. B: Biointerfaces **110**, 178 (2013).